HHS Public Access

Author manuscript

Biomaterials. Author manuscript; available in PMC 2016 December 15.

Published in final edited form as:

Biomaterials. 2016 September ; 102: 259–267. doi:10.1016/j.biomaterials.2016.05.040.

Aligned nanofibrillar collagen scaffolds – Guiding lymphangiogenesis for treatment of acquired lymphedema

Catarina Hadamitzky[a,b], **Tatiana S. Zaitseva**[c], **Magdalena Bazalova-Carter**[d,e], **Michael V. Paukshto**[c], **Luqia Hou**[f,g], **Zachary Strassberg**[g], **James Ferguson**[h], **Yuka Matsuura**[i], **Rajesh Dash**[i], **Phillip C. Yang**[i], **Shura Kretchetov**[j], **Peter M. Vogt**[b], **Stanley G. Rockson**[#i], **John P. Cooke**[#i,l], and **Ngan F. Huang**[#f,g,m,**]

[a]Clinic of Plastic, Esthetic and Hand Surgery, Helios Clinic Hildesheim, Hildesheim 31135, Germany

[b]Clinic of Plastic, Hand and Reconstructive Surgery, Hannover Medical School, Hannover 30625, Germany

[c]Fibralign Corporation, Union City, California 94587, USA

[d]Department of Radiation Oncology, Stanford University, Stanford, California 94305, USA

[e]Department of Physics and Astronomy, University of Victoria, Victoria, British Columbia V8P5C2, Canada

[f]Stanford Cardiovascular Institute, Stanford University, Stanford, California 94305, USA

[g]Center for Tissue Regeneration, Repair and Restoration, Veterans Affairs Palo Alto Health Care System, Palo Alto, California 94304, USA

[h]Surpass Inc., Mountain View, California 94043, USA

[i]Division of Cardiovascular Medicine, Stanford University, Stanford, California 94305, USA

[j]IntraOp Medical Corporation, Sunnyvale, California 94085, USA

[l]Center for Cardiovascular Regeneration, Houston Methodist Research Institute, Houston, Texas 77030, USA

[m]Department of Cardiothoracic Surgery, Stanford University, Stanford, California 94305, USA

[#] These authors contributed equally to this work.

Abstract

Secondary lymphedema is a common disorder associated with acquired functional impairment of the lymphatic system. The goal of this study was to evaluate the therapeutic efficacy of aligned

Correspondence to: Catarina Hadamitzky.

[**]Corresponding author. Department of Cardiothoracic Surgery, 300 Pasteur Drive, Stanford, CA 94305-5407, USA. *E-mail addresses:* ngantina@stanford.edu (N.F.Huang), catarina.hadamitzky@helios-kliniken.de (C.Hadamitzky).

Appendix A. Supplementary data Supplementary data related to this article can be found at http://dx.doi.org/j.biomaterials.

Competing financial interests Fibralign Corporation© produces the aligned nanofibrillar collagen scaffolds we have used in this study. M.V. Paukshto is CTO and T.S. Zaitseva is leading researcher of Fibralign Corporation©. J.P. Cooke and C. Hadamitzky have received subscription rights in Fibralign Corporation©. Other authors declare no competing financial interests.

nanofibrillar collagen scaffolds (BioBridge) positioned across the area of lymphatic obstruction in guiding lymphatic regeneration. In a porcine model of acquired lymphedema, animals were treated with BioBridge scaffolds, alone or in conjunction with autologous lymph node transfer as a source of endogenous lymphatic growth factor. They were compared with a surgical control group and a second control group in which the implanted BioBridge was supplemented with exogenous vascular endothelial growth factor-C (VEGF-C). Three months after implantation, immunofluorescence staining of lymphatic vessels demonstrated a significant increase in lymphatic collectors within close proximity to the scaffolds. To quantify the functional impact of scaffold implantation, bioimpedance was used as an early indicator of extracellular fluid accumulation. In comparison to the levels prior to implantation, the bioimpedance ratio was significantly improved only in the experimental BioBridge recipients with or without lymph node transfer, suggesting restoration of functional lymphatic drainage. These results further correlated with quantifiable lymphatic collectors, as visualized by contrast-enhanced computed tomography. They demonstrate the therapeutic potential of BioBridge scaffolds in secondary lymphedema.

Keywords

Nanofibrillar collagen scaffold; Lymphangiogenesis; Lymphatic vessel regeneration; Lymphedema; VEGF-C; Lymph node transplantation; Porcine lymphedema model; Lymphatic CT-imaging

Introduction

Purposeful growth of vessels and nerves plays a major role in regenerative processes in mammals. In some conditions this growth is impaired, leading to disease perpetuation. Currently, there is no established method to provide mechanical support for the directed growth of vessels or nerves after initial sprouting. We have previously reported, in the context of vascular disease, that parallel-aligned collagen nanofibrillar scaffolds (BioBridge) provide nano-scale spatial guidance cues for alignment and migration of human microvascular blood endothelial cells along the direction of the nanofibrils, as well as induce arteriogenesis in a preclinical model of peripheral arterial disease [1–3].

Acquired (secondary) lymphedema is another pathology directly associated with impaired regeneration of damaged vasculature. This condition leads to accumulation of proteins, cell debris and fluid in the tissues due to the functional impairment of the lymphatic system. It is characterized by chronic swelling that tends to worsen with time [4]. In some cases, it can also be caused by the absence or destruction of lymph nodes. These structures are functionally relevant, as they not only play a fundamental role in immune surveillance but also participate in fluid homeostasis, thereby actively reducing edema [5]. In developed countries, lymphedema often occurs as a consequence of cancer therapeutics. The treatment of many cancers involves surgical extirpation of lymph nodes and/or radiotherapy [6, 7]. It is estimated that 20–50% of these cancer patients develop lymphedema [4, 7, 8]. Present management is palliative and includes lifelong manual lymphatic drainage, compression therapy and, sometimes, wide debulking through liposuction [9]. Secondary lymphedema may occasionally respond to non-palliative surgical interventions. Among several currently

employed treatment procedures, free flaps containing lymph nodes seem to provide clinical benefits [10–12]. Engrafted lymph nodes are potent inducers of lymphangiogenesis [13]. However, in some patients with extensive operative scars, irradiated tissues, or late fibrotic stages of lymphedema, the lymphangiogenic response to vital lymph node flaps can sometimes be insufficient to bridge the scar area and produce a clinical improvement [13].

To address this limitation, we examined the effects of the implantation of aligned nanofibrillar collagen scaffolds in a newly developed porcine model for secondary lymphedema. The purpose of the study was to examine the role of BioBridge scaffolds in facilitating the ingrowth of newly formed lymphatic vessels across the zone of scar tissue. Herein we demonstrate that implantation of the scaffolds, with or without simultaneous transplantation of autologous lymph node fragments, significantly improves lymphatic regeneration in comparison with control interventions.

Materials and methods

2.1. Fabrication and characterization of aligned nanofibrillar collagen scaffolds

BioBridge resorbable collagen scaffolds (Fibralign Corporation, Union City, CA, USA) were produced according to a process based on the technology developed for liquid crystal display manufacturing [14, 15] that is suitable for lyotropic liquid crystal materials, as described previously [2, 3]. In brief, purified monomeric bovine type I collagen solution in a liquid crystal state [16, 17] was sheared onto a plastic substrate [18] to produce one micron thin membrane formed of about 30 nm diameter parallel-aligned fibrils. The membrane was delaminated from the plastic substrate and converted into a scaffold using liquid-air surface tension [19]. Collagen scaffolds were further cross-linked using 0.25 mg 1-ethyl-3-(3-dimethylaminopropyl)-1-carbodiimide hydrochloride (EDC) and 0.28 mg sulfo-N-hydroxysuccinimide (NHS) per mg collagen scaffold, which corresponded to 1 mg/ml EDC per 1.1 mg/ml NHS working concentration, followed by 4 washes in phosphate-buffered saline (PBS) and 2 washes in deionized water [20]. For quantification of scaffold degradation, the scaffolds were crosslinked at 0.2, 0.5, 0.8 and 1 mg/ml EDC concentrations, with NHS concentration adjusted accordingly. Enzymatic degradation of the scaffolds was performed by incubation in bacterial collagenase (50 U/ml) for 4 h. The degraded collagen in solution was quantified by reacting with 2% ninhydrin. The capillarity of the scaffold was measured for 13-mm long samples of BioBridge placed on hydrophobic teflon surface in a horizontal position. A syringe with 25G needle was used to deliver approximately 0.1 mL of green food coloring dye to the end of the scaffolds. Time points of 2 and 4 minutes were taken to analyze how far the dye had traveled along each sample. The capillary propagation of the green coloring dye was measured by camera in green channel with the baseline of the initial white color of the dry BioBridge scaffold.

For *in vitro* studies, primary human microdermal lymphatic endothelial cells (LECs, 0.5×10^6 cells/ml, Lonza, Allendale, NJ, USA) were seeded onto the scaffolds after sterilization using 70% ethanol. Characterization and quality control of these thread-like nanofibrillar collagen scaffolds (12–15 cm long and ~0.3 mm in diameter) was performed using conventional atomic force microscopy and scanning electron microscopy, as described previously [2].

2.2. Heparin conjugation of BioBridge scaffolds

To assess the role of exogenous growth factors attached to the collagen scaffolds in the tissues, a number of scaffolds were first cross-linked and conjugated with heparin following a modified procedure of Steffens *et al.* [21]. Activation of 1 mg heparin was performed using 1 mg of EDC [20] and 1.1 mg NHS (pH 6) during 30 min at room temperature. The pH of this reagent solution was then adjusted to 7.4 with NaOH. It was then added to collagen scaffolds in the proportion of 0.25 mg EDC/NHS reagent solution per 1 mg collagen. Incubation occurred during four hours at room temperature and under gentle shaking. Thereafter, the heparinized collagen scaffolds were washed four times in 24 h with PBS and five times in 24 h with deionized water. The scaffolds were further sterilized by incubation in 70% ethanol for 1 h at room temperature both for the *in vitro* and for the *in vivo* studies.

2.3. VEGF-C attachment to BioBridge scaffolds

To immobilize VEGF-C to heparin, VEGF-C molecules (R&D Systems, Minneapolis, MN, USA) were exposed to the heparin bound on collagen scaffolds. Sterile heparinized scaffolds were incubated in sterile VEGF-C solution (0.5-1.5 μg/ml in PBS for initial studies, and 1.5 μg/ml was selected for subsequent experiments) for 24 h at 4°C [21] and then rinsed three times in PBS. To determine VEGF-C release kinetics, scaffolds conjugated with VEGF-C were whether incubated with 200 μl bacterial collagenase solution (1 U/ml) or with PBS at 37°C. At specific time intervals, the incubation solutions were collected and replaced with fresh aliquots for further incubation. The VEGF-C content in the collected samples was measured using VEGF-C enzyme linked immunosorbent assay (ELISA) according to manufacturer's instructions (R&D Systems).

2.4. Bioactivity of VEGF-C-conjugated BioBridge scaffolds

A modified wound-healing chemotaxis assay was performed to verify the bioactivity of the VEGF-C released from the scaffolds. LECs (Lonza) were cultured to confluence in growth media (EGM-2MV, Lonza) within wound healing chambers having a predefined gap space (Ibidi, Verona, WI, USA), according to our previous studies [22]. Wound healing chambers were removed and the media were changed to basal media (EBM, Lonza) in the presence of 5% fetal bovine serum without growth factor supplement. Sterile 4-cm scaffolds conjugated with VEGF-C (delivering 59.2 ng VEGF-C) or heparin (control) were placed into 400 μl media. Cell migration into the predefined gap was analyzed after 18 hours using Image J (open source, National Institutes of Health, Bethesda, USA). A positive assay control consisted of soluble VEGF-C (100 ng/ml, R&D Systems) added to 400 μl media for the same duration of time ($n \geq 3$).

2.5. Porcine model of secondary lymphedema

All procedures were approved by the Institutional Animal Care and Use Committees at Stanford University (Stanford, CA, USA) and by Surpass - Silicon Valley (Mountain View, CA, USA). Lymphatic stasis and tissue fibrosis was induced in female Yucatan minipigs ($n = 16$, 27 ± 3.3 kg) to simulate the lymphadenectomy and irradiation in human cancer therapeutics. In the anesthetized state, animals had an intradermal injection of 1 ml of 1% methylene blue (Akorn, Lake Forest, IL, USA) into the right paw to allow visualization of

the lymphatics. They then underwent surgical resection of the superficial right inguinal lymph node and of the lymphatic collectors of the right groin. Major lymphatic collectors and superficial blood vessels were ligated. In addition, subcutaneous fatty tissue was resected from the gluteal muscle fascia to the ventrocranial iliac spine, sparing the dermal blood-vascular plexus to prevent skin necrosis. This resection created a gap in the groin subcutaneous fatty tissue of about 2 cm. Next, a resection of the right popliteal lymph node, its surrounding collectors, and immediately adjacent fatty tissue was performed. In both sites, a thorough electrocoagulation of the lymphatic collectors and superficial blood vessels was performed with bipolar tweezers before subcutaneous wound closure with 2–0 PDS inverted single knot sutures (Ethicon/J&J, Guaynabo, Puerto Rico). The skin was then closed in both sites with 3-0 resorbable monofilament (Ethicon/J&J), followed by application of a transparent waterproof wound dressing (Tegaderm transparent film dressing, 3M Health Care, St. Paul, MN, USA) and Mastisol liquid skin adhesive (Ferndale Laboratories, Ferndale, MI, USA). Animals were allowed to recover for 14 days to ensure complete wound closure prior to undergoing irradiation procedure.

2.6. Irradiation of the groin

To simulate the cancer therapeutic irradiation procedure, a single dose of 15 Gy (Mobetron, IntraOp Medical, Sunnyvale, CA, USA) was delivered with a 6 MeV electron beam to the right groin to a depth of 3 cm. After a CT-imaging of an average sized animal to support the general planning of the radiation, special care was taken to exclusively expose the right groin in an area of 8 × 15 cm, without compromising the left hind limb (control). A 1 cm thick bolus was applied ventrally to increase the surface dose delivered to the superficial layers of the treatment area (Suppl. Fig. 1).

2.7. Scaffold implantation in vivo

At the initiation of the study, pre-operated and pre-irradiated animals were randomized into three groups:

1) Experimental treatment groups received BioBridge scaffolds, with or without autologous avascular lymph node fragment transfer (BioBridge ± LNT, n=8).

2) The first post-surgical control group was untreated (Untreated, n=4).

3) The second control treatment group received BioBridge scaffolds conjugated with VEGF-C (BioBridge + VEGF-C, n=4), utilizing the rationale that uniform expression of VEGF-C throughout the length of the scaffold would cancel the directional signalling of the growth factor and thereby mitigate the growth-stimulating effect of the scaffold.

In all animal subjects, the contralateral hind limb (left) was additionally used as an intra-individual normal control (absence of any intervention) for the pre-operated and pre-irradiated right hind limb.

A schematic overview and peri-operative images of the scaffold implantation procedure are shown in Suppl. Fig. 2. In the anesthetized state, subjects were injected intradermally with 1 ml of methylene blue into the right paw to visualize the lymphatic collectors. Two small

incisions were made cranially and caudally to the prior lymphatic resection/irradiation area in the right groin. Between these two incisions, a subcutaneous tunnel that followed the axis of the right limb was carefully created to embed the transplants in the irradiated area (~10–12 cm in length-). Half of the animals in the experimental treatment group each received ten (10) unsupplemented BioBridge threads (~16 cm in length per scaffold), inserted subcutaneously in the right groin. Proximally, the embedded thread-like scaffolds were sutured to the surrounding connective tissue with non-resorbable 6-0 prolene sutures (Ethicon/J&J). Distally, five threads were microsurgically sutured to methylene blue stained lymphatic collectors with 10–0 ethilon sutures (Ethicon/J&J). Since BioBridge threads do not have a patent lumen, the connection to stained lymphatic collectors was performed with an extraluminal single stitch. The other five threads were slightly unfolded distally and fixed with a single 6-0 prolene stitch (Ethicon/J&J) within the tissue presenting no visible collectors in the vicinity. Also in the experimental treatment group, another cohort received each five (5) unsupplemented BioBridge and five (5) VEGF-C-conjugated BioBridge scaffolds (~16 cm in length per scaffold), transferred together with autologous lymph node fragments [23]. Here, two fragments from the left inguinal lymph node were harvested and implanted equidistantly from the proximal and distal thread ends on the right side, and fixed to the superficial abdominal muscle fascia with non-resorbable prolene 3-0 sutures (Ethicon/J&J).

The untreated surgical control group underwent initial resection of the lymphatic system in the right groin and right popliteal area followed by radiation three months before the start of the study, and thereafter received no additional treatment.

The exogenous VEGF-C control group received five (5) unsupplemented and five (5) VEGF-C-conjugated BioBridge scaffolds (~16 cm in length per scaffold) with an average amount of total VEGF-C delivered of ~1 μg per animal. Animals were allowed to recover and were monitored for wound healing problems and seromata.

2.8. Histological evaluation

At the final three-month time point of the study, the subjects were euthanized after imaging and harvesting of the tissue samples from the implantation site. Following immediate fixation in 10% buffered formalin, samples were embedded in paraffin, and 6 μm transverse sections were cut for routine hematoxylin and eosin (H&E) evaluation. For immunofluorescence staining of lymphatic collectors and blood vessels, the paraffin-embedded tissue sections were first de-paraffinized and rehydrated before undergoing antigen retrieval at high heat (1x Reveal, Biocare Medical, Concord, CA, USA). Tissues were incubated with antibody directed against lymphatic endothelial marker (LYVE-1, Abcam, Cambridge, MA, USA), followed by incubation with Alexafluor-594-conjugated secondary antibody (Life Technologies, Carlsbad, CA, USA). Additionally, the slides were incubated with vascular smooth muscle marker smooth muscle α-actin (α-SMA, Sigma) as well as with Alexafluor-488-conjugated secondary antibody (Life Technologies). Finally, the nuclei were visualized using Hoechst 33342 dye (Life Technologies).

2.9. Quantification of lymphatic and blood vessel regeneration

To quantify the lymphatic and blood vessel regeneration within the immediate vicinity of the scaffold, the immunofluorescence sections were imaged under a confocal microscope (LSM 710, Carl Zeiss). Regional rings were established by measuring radial distances (0 μm; 50 μm; 100 μm and 150 μm) surrounding the periphery of the scaffold using ImageJ software (US National Institutes of Health). Within each ring, the number of lymphatic collectors (α-SMA$^+$/LYVE1$^+$)[24] and blood vessels (α-SMA$^+$/LYVE1$^-$) were counted and then expressed in the form of density (#/mm^2) by normalizing to the area of each ring. As an internal negative control for the regenerative effects of the scaffold, lymphatic and blood vascular densities were similarly quantified for tissue regions > 2000 μm away from the scaffolds, also within the pre-operated and pre-irradiated tissue.

2.10. Bioimpedance (BI) measurements

At the starting and final time points of the study (0 and 3 months, respectively), extracellular fluid volume in both hind limbs was quantified by multi-frequency BI analysis [25] using a well-established BI device (ImpediVET, Carlsbad, CA, USA) [26] to measure the BI at low frequency current on both hind limbs. Bioimpedance spectroscopy (BIS) is one of the few techniques of body composition analysis which differentiates the extracellular fluid compartment from the total limb volume [27]. The use of BIS for clinical monitoring of the risk of lymphedema and of lymphedema progression is under increasingly wide application and has been validated in numerous prospective clinical studies [28, 29]. Multi-frequency BI analysis is based on the fact that the resistance to the flow of electric current through the body is inversely proportional to the volume of fluid in the tissue. Nearly all of the current that passes through the extracellular fluid is of low frequency [25]. At higher frequencies, the current passes through both the extracellular and intracellular fluid as the resistance of the cell membranes decreases [30]. In lymphedema, it is excessive interstitial fluid that accumulates. In this case, the tissue bioimpedance at low-frequency current decreases, since the passage of electric current is facilitated when the tissue environment has more water.

To collect these data, each animal was placed on a plastic table, the hind limbs shaved over the metatarsal bones and thoroughly cleaned with 70% ethanol. Thereafter, electrodes with film contacts were carefully placed on the dry skin (Suppl. Fig. 3). BI measurements were recorded, and the ratio between the impedance of the right hind limb (therapy) and of the left hind limb (control) calculated. This ratio reflects the intra-individual difference in extracellular fluid volumes in the limbs. In each subject, the baseline bioimpedance ratio was recorded [31] and repetitive re-measurement was utilized to monitor disease progression *in vivo* during the course of the study.

2.11. CT imaging of the lymphatic vessels in both hind limbs

Both at the starting and final time points of the study, a contrast-enhanced CT-scan was performed under general anesthesia. To visualize the lymphatic system by intradermal injection of iodine contrast (Optiray™, Covidien, Hazelwood, MO, USA), a pearl bracelet distribution at 3 cm above the area of transition between the hoof and the skin of the right hind limb was used. After the first imaging session, in which eight CT datasets of the right limb were acquired during a seven-minute interval, the same contrast injection procedure

was performed on the left hind paw. Another series of images was collected for three minutes. CT data was evaluated by a blinded reader, and the number of visualized lymphatic collectors in the treatment area was recorded for each subject. The number of collectors in the groin area of the healthy control limbs on the left side was also quantified.

2.12. Statistical analysis

All data are shown as mean ± standard error of mean. Statistical comparisons between two time points within each treatment were performed by a Student's paired t-test. Statistical comparisons between more than two time points within each treatment were performed by a repeated measures analysis of variance (ANOVA) with Holm's adjustment. Comparison of three or more groups was performed by a one-way ANOVA with Holm's adjustment. Statistical significance was accepted at $p < 0.05$.

3. Results

3.1. Characterization of aligned nanofibrillar scaffolds

The thread-like BioBridge nanofibrillar scaffolds were approximately 0.3 mm in diameter (Fig. 1A), and were composed of aligned nanofibrils of approximately 30 nm diameter, as shown by AFM and SEM images of the scaffold surface (Fig. 1B–C). Cross-sectional imaging of the BioBridge scaffolds demonstrated a porous structure, in which the pores maintained parallel-aligned nanofibril orientation (Fig. 1D–E). BioBridge scaffolds were degraded by collagenase, with a degradation rate that correlated with the degree of cross-linking (Suppl Fig. 4A), confirming that the zero-length EDC crosslinking enables effective control of BioBridge degradation without introducing any additional material [32, 33]. The 1 mg/ml EDC concentration was selected for scaffold preparation, in accordance with the previous studies [2, 3]. The porous structure of BioBridge provided enabled capillary flow along the length of the thread-like scaffold (Suppl Fig, 4B–C). *In vitro* studies demonstrated that the BioBridge scaffolds morphologically reorganized LEC cytoskeletal assembly along the direction of the collagen nanofibrils (Suppl. Fig. 5), in accordance with our previous findings using microvascular endothelial cells [3].

3.2. Conjugation of VEGF-C with aligned nanofibrillar scaffolds

To examine the relationship between VEGF-C loading and release profile, scaffolds were incubated with VEGF-C ranging from 0.5-1.5 μg/ml for 24 h. Scaffolds loaded with 1.0 or 1.5 μg/ml of protein showed similar levels of VEGF-C release (~15 ng per cm sample) after incubation in collagenase for 3 days, which was significantly greater than the release from scaffolds loaded with 0.5 μg/ml ($p < 0.05$; $n \geq 3$; Suppl. Fig. 6A). Based on these observations, we selected the 1.5 μg/ml concentration for subsequent *in vitro* and *in vivo* testing. For the 1.5 μg/ml concentration of loaded VEGF-C, the amount of VEGF-C retained in the scaffold was 9.7 ± 1.3% of the total VEGF-C amount in the conjugation reaction (255 ng VEGF-C per mg scaffold). Furthermore, the release profile of VEGF-C over a 6-day period demonstrated that VEGF-C release in a saline solution was significantly lower than that in the presence of collagenase at all time points ($p < 0.001$; $n \geq 3$, Suppl. Fig. 6B) and comprised 11% of the total VEGF-C released after collagenase treatment, suggesting that scaffold degradation may be needed for complete growth factor release.

3.3. Bioactivity assay of conjugated BioBridge scaffolds

To validate the bioactivity of the VEGF-C-conjugated BioBridge scaffolds, we performed a modified wound healing scratch assay, in which a pre-formed gap was created in a monolayer of human LECs. The media (400 μl) were supplemented with VEGF-C scaffolds (4 cm total length, delivering 14.8 ng/cm × 4 cm = 59.2 ng VEGF-C, of which ~75% was released within 24 h) or soluble VEGF-C (40 ng), and cell migration into the gap was then quantified after 18 h. As shown in Suppl. Fig. 6 C–D, the migration of LECs into the gap was more than 50% greater in samples treated with VEGF-C-conjugated scaffolds than heparin-conjugated scaffolds (control), reaching similar levels to that of samples treated with soluble VEGF-C ($p < 0.05$, $n \geq 3$).

Together, these results demonstrated that 1) BioBridge scaffolds are composed of aligned nanofibrils that are able to guide the orientation of LECs and; 2) VEGF-C-conjugated scaffolds are able to induce LEC migration into a pre-formed gap.

3.4. Characterization of the lymphedema model

We developed a porcine chronic lymphedema model to evaluate whether BioBridge scaffolds, also in conjunction with endogenous (lymph node fragment transfer) or exogenous VEGF-C release, could bridge the area of lymphatic obstruction by providing physical and chemical guidance cues, as shown schematically in Fig. 2A. The porcine model was developed by meticulous resection of the lymphatic system of one hind limb and subsequent radiotherapy. Animals at the starting time point were categorized as having lymphedema based on a BI ratio ≥ 1.05 [30, 31], as well as on the depletion (# ≤ 2) of lymphatic collectors by CT imaging in the operated right leg (Fig. 2B). MRI imaging further confirmed the incidence of lymphedema based on asymmetric subcutaneous fluid accumulation or dermal backflow (see Fig. 2C arrowheads) [34] as an indirect sign of lymphedema at the 0 and 3 month time point (Fig. 2C)[4, 7].

3.5. Histological Analysis of Lymphatic Regeneration

At 3 months after implantation of BioBridge scaffolds, sections of subcutaneous tissue were histologically assessed by hematoxylin and eosin staining. Whereas the untreated control animals developed fibrous scar tissue (Suppl. Fig. 7A), the animals that received either BioBridge±LNT or BioBridge+VEGF demonstrated biocompatibility and integration of the nanofibrillar collagen scaffold into the irradiated tissues (Suppl. Fig. 7B–C). The partially degraded scaffolds could be visualized as ribbon-like bands, as denoted by arrows. Cellular infiltration was observed to be abundant in the inner space throughout the scaffold, with minimal evidence of inflammation (Suppl. Fig. 7B–C).

We next quantified the lymphatic density at both local (0, 50, 100 and 150 μm) and distant (>2000μm) radial distances away from the scaffolds. The aim was to verify the specificity of increased vascular regeneration due to scaffold treatment, rather than a non-specific inflammatory response due to the creation of the subcutaneous tunnel, that would be observed even at regions distant from the scaffold. To do so, rings were drawn at radial distances of 0, 50, 100, 150, and >2000 μm away from the periphery of the scaffold (Suppl. Fig. 8). Within each ring, the density of lymphatic collectors (α-SMA$^+$/LYVE1$^+$) [24] and

blood vessels (α-SMA$^+$/LYVE1$^-$) were quantified. In the treatment group receiving BioBridge with or without lymph node fragment transfer, immunofluorescence staining for lymphatic collectors (LYVE1$^+$/α-SMA$^+$) revealed a significantly higher density of these vessels in the proximity of the BioBridge scaffold (e.g. 27.3 ± 4.5/mm^2 (100 μm from the scaffold)), when compared to the surrounding irradiated tissue (1.7 ± 0.6/mm^2 (2000 μm), $p < 0.05$) or to the untreated group (0.7 ± 0.22/mm^2, $p < 0.05$) (Fig. 3A,C). Similarly, animals receiving BioBridge combined with VEGF-C (exogenous VEGF-C control) also showed a significantly higher density of lymphatic collectors ($p < 0.05$) in the vicinity of scaffolds (e.g. 30.1 ± 9.8/mm^2 (50 μm), 26.4 ± 6.7/mm^2 (100 μm)), when compared to the untreated group or surrounding irradiated tissue. In all BioBridge implanted groups, an increased lymphatic vessel density was observed in close proximity to the scaffold, but neither in the remote irradiated tissue (>2000μm) nor in the untreated control group, suggesting that the scaffolds were specifically responsible for the local increase in lymphatic vessel density.

In addition to lymphatic vessel density, we also quantified vascular density, based on LYVE1$^-$/α-SMA$^+$ staining. In the experimental treatment group that received BioBridge, with or without lymph node transfer, vascular density was significantly higher ($p < 0.05$) in close proximity to the scaffold (e.g. 31.6 ± 2.75/mm^2 (50 μm), 38.7 ± 6.38/mm^2 (100 μm)), when compared to the untreated control group (6.5 ± 1.12/mm^2) (Fig. 3B,D). Interestingly, the balance between the lymphatic and blood vessels in the vicinity of the scaffold was shifted toward lymphatics for all treatment groups, as shown by the increase in the lymphatic fraction of the total (lymphatic + blood) microvascular density within a 100 μm distance from the scaffolds (Fig. 3E, $p < 0.05$).

3.6. Quantification of lymphatic function by analysis of bioimpedance ratio

Since histological analysis provided structural evidence of reparative lymphangiogenesis, we decided that it would be important to determine whether the therapeutic interventions with the Biobridge provided functional improvement based upon the lymphangiogenic response. Accordingly we compared the changes in mean BI ratio for each group prior to initiation of the therapy and at the final time point (at three months following therapeutic intervention) (Fig. 4). In the untreated control group, the BI showed no significant change between the two time points. In contrast, in the experimental treatment group, implantation of BioBridge, with or without lymph node transfer, ameliorated tissue edema, as evidenced by a significant reduction in the BI ratio, this being the surrogate measure of extracellular fluid volume ($p < 0.05$). In the exogenous VEGF-C control group, the subjects experienced worsening of edema, with a change in BI from 0.97±0.10 to 1.1 ± 0.6 ($p < 0.05$). Each group of BioBridge scaffold recipients demonstrated histological evidence of increased lymphatic vascular density (Fig. 3), but only the experimental treatment group demonstrated functional amelioration (Fig. 4). The absence of functional improvement in the exogenous VEGF-C/ Biobridge control group, despite histological evidence of enhanced lymphatic vascular density, suggests that the functional amelioration that accompanies the implantation of the Biobridge can be mitigated through the loss of directionally appropriate growth factor signalling. The latter appears to be necessary for the restoration of normal lymphatic anatomy and function.

3.7. Quantification of lymphatic regeneration by CT imaging

CT imaging of the limb following contrast injections of the lymphatic vessels was used to verify the BI data and to identify the lymphatic collecting vessels with a size sufficient for CT resolution. For each treatment group, we quantified the collector ratio [(identified collectors in the diseased (right) limb)/(identified collectors in the healthy (left) limb) × 100%] at baseline (before treatment) and at three months after treatment (Suppl. Fig. 9 & Table 1). In the untreated control group, there were no significant changes in CT-imaged lymphatic collectors. In contrast, the subjects that received BioBridge scaffolds, with or without autologous avascular lymph node fragment transfer, showed an increase of 15% in CT-detectable *de novo* lymphatic collectors. The exogenous VEGF-C controls demonstrated a 48% decrease in CT-detectable lymphatic collectors, concurrent with the bioimpedance data.

In summary, histological, functional and imaging analyses all suggest that use of the BioBridge, with or without concomitant lymph node transfer, was responsible for the therapeutic response of functional lymphatic regeneration in this surgical model of acquired lymphedema.

4. Discussion

Various scaffolds have been used historically in an attempt to restore lymphatic function in lymphedema patients. In 1908, W. S. Handley proposed using sterile silk sutures as artificial lymphatic conduits [35]. He showed that when these silk threads were implanted subcutaneously into the affected arms, they helped drain lymphatic fluid by means of capillary action. While there was an initial beneficial effect, the silk threads ultimately created foreign body reactions that reduced the lymphatic fluid drainage within a short time after implantation and created other complications, including infection. Later, a similar approach was initiated that utilized a wicking Teflon multifilament material instead of silk [36]. It was reported that lymphedema relief lasted for some time before the Teflon structure succumbed to fibrotic encapsulation. While these results were not sufficiently satisfactory to be used clinically as a viable treatment option, they confirmed that Handley's concept of creating an artificial lymphatic channel could produce acute relief from lymphedema.

Recent studies have shown that interstitial flow is a major factor in the formation of new lymphatic capillaries [37]. Directional interstitial flow precedes the formation of lymphatic vessels in the flow direction. The BioBridge scaffold may fact by inducing capillary flow (Suppl., Fig. 4B–C), and therefore it may provide both acute relief from swelling as well as a favorable condition for lymphangiogenesis. BioBridge provides a suitable environment for endothelial cells. In particular, the scaffold has been extensively tested and optimized in the murine hind limb model as a mean to induce directional angiogenesis and arteriogenesis [2, 3]. The aligned nanofibrillar scaffold preserves endothelial cell phenotype even in ischemic conditions and provides the substrate for endothelial cell alignment and migration along the collagen fibrils [3, 38, 39]. The current results suggest that BioBridge scaffolds may provide a potent stimulus to lymphatic regeneration.

The scarcity of both lymphatic and blood micro-vasculature in the area of obstruction (both in control animals and at remote-from-scaffold sites in all treated animals) indicates that the procedures employed to create the lymphedema model did eliminate the vast majority of lymphatic collectors, as intended. Therefore, increased lymphatic (and blood) vascular densities detected per confocal microscopy in the vicinity of the scaffold, when compared to untreated control tissue, strongly suggest that the vessels in this area are largely newly formed. It is noteworthy that, while both lymphangiogenesis and angiogenesis occurred in close proximity to the scaffold in all treatment groups, the lymphangiogenic effect eclipsed the angiogenic response in this same area, suggesting that BioBridge may preferentially target lymphangiogenesis. In the application of this model to our scientific question regarding the utility of Biobridge scaffolds in lymphatic repair, we did not choose to intercompare the two scaffold categories, because this large animal study was underpowered to provide a valid intercomparison. Our primary intent with this investigation was to study the impact of the Biobridge on reparative lymphangiogenesis, which occurred with or without the addition of lymph node supplementation.

A major limiting factor in surgical research has been the lack of large animal models that mimic lymphedema in humans [40]. Our current large animal model of secondary lymphedema seems to be appropriate for surgical research purposes. A disadvantage of this large animal model was the relatively long time frame necessary for the establishment of chronic lymphedema features in the tissues. The associated challenges constrained the number of animals and observations. In this model, the incidence of lymphedema parallels what is seen in human post-surgical lymphedema [41]. The consistency of the intra-individual observations by bioimpedance, contrast-MRI (Suppl. Methods) and contrast-CT validate the latter as a reliable three-dimensional depiction of macroscopic lymphatic collectors and lymph nodes.

The results associated with the exogenous VEGF-C control group suggest that coating the BioBridge with VEGF-C [42], a potent inducer of lymphatic vessel sprouting [43], serves to impede rather than to stimulate the functional therapeutic response. The development of nonfunctional vascular proliferation in the presence of VEGF-C-coated threads is reminiscent of the aberrant blood vessel angiogenesis with high local expression of VEGF-A [44] as well as the pathological lung lymphangiogenesis that occurs in the presence of high levels of VEGF-D [45]. Nevertheless, it is plausible to conjecture that the negative observations were not instigated by the growth factor *per se*, but from the imposed absence of a directional chemical gradient of VEGF-C. In the presence of enhanced concentrations of exogenous VEGF-C distributed uniformly throughout the length of the scaffold, the directionality of required lymphatic regeneration was obscured, leading to an ineffectual form of regenerative lymphangiogenesis.

One of the changes observed in the subcutaneous tissue of human patients after radiotherapy is a unidirectional alignment of dermal collagen fibres [46]. These ultra-structural changes are not only responsible for the loss of tissue elasticity, but also constitute a structural barrier [46]. Guiding cell migration by providing a biocompatible three-dimensional anchoring structure in the form of a collagen scaffold would be theoretically advantageous, particularly in post-surgical and irradiated tissues. In the experimental treatment group, implantation of

collagen scaffolds supported lymphatic regeneration and produced consistent reduction of edema fluid. Furthermore, concurrent transplantation of lymph node fragments, known to produce endogenous VEGF-C, had no adverse effects, confirming what has previously been observed in this context [47]. In this study, the transplanted lymph node fragments showed only small areas of cellular organization (data are not presented), corresponding to zones of adequate organ function [48]. Scattered functional areas within transplanted nodes have been described by others [49] and suggest a premature interruption of the regeneration process [43] within the subcutaneous fat [50]. In contrast, in young mice the time course of lymphatic reconstitution after tissue transplantation is very rapid [51]. This phenomenon indicates that longer periods of follow-up may be required for the study of lymphatic regeneration in large animals, if they are to serve as models for human disease and therapeutics [10]. Nevertheless, despite incomplete regeneration of the lymph node fragments, the addition of these nodal foci seemed to act synergistically with the implanted subcutaneous scaffolds, leading to the improvement in pathological tissue edema through the stimulated growth of new lymphatic collectors in the area of obstruction.

For delivery of the BioBridge scaffold as a therapeutic treatment for lymphedema, we acknowledge that the surgical implantation approach utilized in the porcine model would be considered invasive for human subjects. For this reason we envision developing a minimally invasive implantation procedure in which the scaffolds could be delivered through an area of lymphatic obstruction with the use of tunnelling surgical devices. In addition, future studies to elucidate the basic signalling mechanism by which BioBridge induces lymphatic regeneration are warranted.

Conclusion

In conclusion, this study represents the first demonstration of effective therapeutic lymphangiogenesis induced by the implantation of nanofibrillar scaffolds. Implantation of the collagen scaffolds enhances histologically-defined lymphatic vessel density in the vicinity of the scaffolds in all recipient groups. In our study, the experimental treatment group that received BioBridge scaffolds, with or without lymph node transfer, experienced a functional improvement in concert with imaging and histological evidence of therapeutic lymphangiogenesis. Therefore, the use of aligned nanofibrillar collagen scaffolds seems to have a potential application in providing mechanical support for directed lymphangiogenesis in secondary lymphedema.

Supplementary Material

Refer to Web version on PubMed Central for supplementary material.

Acknowledgements

The authors thank Greg King for the logistical support, David McMurtry for the assistance in the creation of the collagen scaffolds, Steve Sawamura for running the ELISA, Jennifer Lyons for technical assistance with the animal study and Lydia-Marie Joubert for scanning electron microscopy analysis.

This work was supported partially by grants from the US AMRMC (W81XWH-12-C-0111) and NSF (1249008) to MVP, and a grant from the NIH (R01HL127113) to NFH.

The funders had no role in study design, data collection and analysis, decision to publish or preparation of the manuscript.

References

[1]. Lai ES, Anderson CM, Fuller GG. Designing a tubular matrix of oriented collagen fibrils for tissue engineering. Acta Biomater. 2011; 7(6):2448–2456. [PubMed: 21414424]

[2]. Nakayama KH, Hong G, Lee JC, Patel J, Edwards B, Zaitseva TS, et al. Aligned-braided nanofibrillar scaffold with endothelial cells enhances arteriogenesis. ACS Nano. 2015; 9(7): 6900–6908. [PubMed: 26061869]

[3]. Huang NF, Okogbaa J, Lee JC, Jha A, Zaitseva TS, Paukshto MV, et al. The modulation of endothelial cell morphology, function, and survival using anisotropic nanofibrillar collagen scaffolds. Biomaterials. 2013; 34(16):4038–4047. [PubMed: 23480958]

[4]. DiSipio T, Rye S, Newman B, Hayes S. Incidence of unilateral arm lymphoedema after breast cancer: A systematic review and meta-analysis. Lancet Oncol. 2013; 14(6):500–515. [PubMed: 23540561]

[5]. Mortimer PS, Rockson SG. New developments in clinical aspects of lymphatic disease. J Clin Invest. 2014; 124(3):915–921. [PubMed: 24590276]

[6]. Miller CL, Specht MC, Skolny MN, Horick N, Jammallo LS, O'Toole J, et al. Risk of lymphedema after mastectomy: Potential benefit of applying acosog z0011 protocol to mastectomy patients. Breast Cancer Res Treat. 2014; 144(1):71–77. [PubMed: 24500108]

[7]. Rasmusson E, Gunnlaugsson A, Blom R, Bjork-Eriksson T, Nilsson P, Ahlgen G, et al. Low rate of lymphedema after extended pelvic lymphadenectomy followed by pelvic irradiation of node-positive prostate cancer. Radiat Oncol. 2013:8271.

[8]. Rockson SG, Rivera KK. Estimating the population burden of lymphedema. Ann N Y Acad Sci. 2008:1131147–154.

[9]. Brorson H. Liposuction normalizes - in contrast to other therapies - lymphedema-induced adipose tissue hypertrophy. Handchir Mikrochir Plast Chir. 2012; 44(6):348–354. [PubMed: 23283813]

[10]. Becker C, Assouad J, Riquet M, Hidden G. Postmastectomy lymphedema: Long-term results following microsurgical lymph node transplantation. Ann Surg. 2006; 243(3):313–315. [PubMed: 16495693]

[11]. Sapountzis S, Singhal D, Rashid A, Ciudad P, Meo D, Chen HC. Lymph node flap based on the right transverse cervical artery as a donor site for lymph node transfer. Ann Plast Surg. 2013:73398–401.

[12]. Raju A, Chang DW. Vascularized lymph node transfer for treatment of lymphedema: A comprehensive literature review. Ann Surg. 2014

[13]. Saaristo AM, Niemi TS, Viitanen TP, Tervala TV, Hartiala P, Suominen EA. Microvascular breast reconstruction and lymph node transfer for postmastectomy lymphedema patients. Ann Surg. 2012; 255(3):468–473. [PubMed: 22233832]

[14]. Bobrov Y, Fennell L, Lazarev P, Paukshto M, Remizov S. Manufacturing of a thin-film lcd. J Soc Inf Display. 2002:10317–321.

[15]. Paukshto M, Fuller G, Michailov A, Remizov S. Optics of sheared liquid-crystal polarizer based on aqueous dispersion of dichroic-dye nano-aggregates. J Soc Inf Display. 2005:13765–772.

[16]. Giraud-Guille MM, Mosser G, Belamie E. Liquid crystallinity in collagen systems in vitro and in vivo. Current Opinion in Colloid & Interface Science. 2008:13303–313.

[17]. Muthusubramaniam L, Peng L, Zaitseva T, Paukshto M, Martin GR, Desai TA. Collagen fibril diameter and alignment promote the quiescent keratocyte phenotype. J Biomed Mater Res A. 2012; 100(3):613–621. [PubMed: 22213336]

[18]. McMurtry, D.; Paukshto, M.; Bobrov, Y. A liquid film applicator assembly and rectilinear shearing system incorporating the same. US Patent 20078028647.

[19]. Paukshto, MV.; McMurtry, DH.; Martin, GR.; Zaitseva, T.; Bobrov, YA. Biocomposites and methods of making the same. US Patent 20098513382.

[20]. Wissink MJ, van Luyn MJ, Beernink R, Dijk F, Poot AA, Engbers GH, et al. Endothelial cell seeding on crosslinked collagen: Effects of crosslinking on endothelial cell proliferation and functional parameters. Thrombosis & Haemostasis. 2000; 84(2):325–331. [PubMed: 10959708]

[21]. Steffens GC, Yao C, Prevel P, Markowicz M, Schenck P, Noah EM, et al. Modulation of angiogenic potential of collagen matrices by covalent incorporation of heparin and loading with vascular endothelial growth factor. Tissue Eng. 2004; 10(9–10):1502–1509. [PubMed: 15588409]

[22]. Huang NF, Dewi RE, Okogbaa J, Lee JC, Jalilrufaihah A, Heilshorn SC, et al. Chemotaxis of human induced pluripotent stem cell-derived endothelial cells. Am J Transl Res. 2013; 5(5):510–520. [PubMed: 23977410]

[23]. Hadamitzky C, Blum KS, Pabst R. Regeneration of autotransplanted avascular lymph nodes in the rat is improved by platelet-rich plasma. J Vasc Res. 2009; 46(5):389–396. [PubMed: 19155630]

[24]. Ichise T, Yoshida N, Ichise H. Fgf2-induced ras-mapk signalling maintains lymphatic endothelial cell identity by upregulating endothelial-cell-specific gene expression and suppressing tgfbeta signalling through smad2. J Cell Sci. 2014; 127(Pt 4):845–857. [PubMed: 24357720]

[25]. Thomas BJ, Ward LC, Cornish BH. Bioimpedance spectrometry in the determination of body water compartments: Accuracy and clinical significance. Applied Radiation & Isotopes. 1998; 49(5–6):447–455. [PubMed: 9569513]

[26]. Ward LC, Czerniec S, Kilbreath SL. Operational equivalence of bioimpedance indices and perometry for the assessment of unilateral arm lymphedema. Lymphat Res Biol. 2009; 7(2):81–85. [PubMed: 19522677]

[27]. Smoot BJ, Wong JF, Dodd MJ. Comparison of diagnostic accuracy of clinical measures of breast cancer-related lymphedema: Area under the curve. Arch Phys Med Rehabil. 2011; 92(4):603–610. [PubMed: 21440706]

[28]. Feldman S, Bansil H, Ascherman J, Grant R, Borden B, Henderson P, et al. Single institution experience with lymphatic microsurgical preventive healing approach (lympha) for the primary prevention of lymphedema. Ann Surg Oncol. 2015; 22(10):3296–3301. [PubMed: 26202566]

[29]. Rockson SG. Detecting lymphedema: Bioimpedance spectroscopy and the tissue dielectric constant. Lymphat Res Biol. 2015; 13(3):169. [PubMed: 26359689]

[30]. Cornish B. Bioimpedance analysis: Scientific background. Lymphat Res Biol. 2006; 4(1):47–50. [PubMed: 16569208]

[31]. Svensson BJ, Dylke ES, Ward LC, Kilbreath SL. Segmental impedance thresholds for early detection of unilateral upper limb swelling. Lymphat Res Biol. 2015 not availableahead of print. doi:10.1089/lrb.2013.0050.

[32]. Friess W. Collagen--biomaterial for drug delivery. Eur J Pharm Biopharm. 1998; 45(2):113–136. [PubMed: 9704909]

[33]. Yao C, Markowicz M, Pallua N, Noah EM, Steffens G. The effect of cross-linking of collagen matrices on their angiogenic capability. Biomaterials. 2008; 29(1):66–74. [PubMed: 17935778]

[34]. Lu Q, Delproposto Z, Hu A, Tran C, Liu N, Li Y, et al. Mr lymphography of lymphatic vessels in lower extremity with gynecologic oncology-related lymphedema. PLoS One. 2012; 7(11):e50319. [PubMed: 23209708]

[35]. Handley WS. Two cases of lymphangioplasty for the brawny arm of breast cancer. Proc R Soc Med. 1908; 1(Clin Sect):186–190. [PubMed: 19972723]

[36]. Silver D, Puckett CL. Lymphangioplasty: A ten year evaluation. Surgery. 1976; 80(6):748–755. [PubMed: 1006523]

[37]. Boardman KC, Swartz MA. Interstitial flow as a guide for lymphangiogenesis. Circ Res. 2003; 92(7):801–808. [PubMed: 12623882]

[38]. Lai ES, Huang NF, Cooke JP, Fuller GG. Aligned nanofibrillar collagen regulates endothelial organization and migration. Regen Med. 2012; 7(5):649–661. [PubMed: 22954436]

[39]. Nakayama KH, Surya VN, Gole M, Walker TW, Yang W, Lai ES, et al. Nanoscale patterning of extracellular matrix alters endothelial function under shear stress. Nano Lett. 2016; 16(1):410–419. [PubMed: 26670737]

[40]. Hadamitzky C, Pabst R. Acquired lymphedema: An urgent need for adequate animal models. Cancer Res. 2008; 68(2):343–345. [PubMed: 18199525]

[41]. Monleon S, Murta-Nascimento C, Bascuas I, Macia F, Duarte E, Belmonte R. Lymphedema predictor factors after breast cancer surgery: A survival analysis. Lymphat Res Biol. 2015 not availableahead of print. doi:10.1089/lrb.2013.0042.

[42]. Helotera H, Alitalo K. The vegf family, the inside story. Cell. 2007; 130(4):591–592. [PubMed: 17719536]

[43]. Tammela T, Saaristo A, Holopainen T, Lyytikka J, Kotronen A, Pitkonen M, et al. Therapeutic differentiation and maturation of lymphatic vessels after lymph node dissection and transplantation. Nat Med. 2007; 13(12):1458–1466. [PubMed: 18059280]

[44]. von Degenfeld G, Banfi A, Springer ML, Wagner RA, Jacobi J, Ozawa CR, et al. Microenvironmental vegf distribution is critical for stable and functional vessel growth in ischemia. Faseb J. 2006; 20(14):2657–2659. [PubMed: 17095533]

[45]. McCormack FX, Inoue Y, Moss J, Singer LG, Strange C, Nakata K, et al. Efficacy and safety of sirolimus in lymphangioleiomyomatosis. N Engl J Med. 2011; 364(17):1595–1606. [PubMed: 21410393]

[46]. Iwahira Y, Nagase T, Nakagami G, Huang L, Ohta Y, Sanada H. Histopathological comparisons of irradiated and non-irradiated breast skin from the same individuals. J Plast Reconstr Aesthet Surg. 2012; 65(11):1496–1505. [PubMed: 22721976]

[47]. Honkonen KM, Visuri MT, Tervala TV, Halonen PJ, Koivisto M, Lahteenvuo MT, et al. Lymph node transfer and perinodal lymphatic growth factor treatment for lymphedema. Ann Surg. 2013; 257(5):961–967. [PubMed: 23013803]

[48]. Victora GD. Stop, go, and evolve. Science. 2013; 342(6163):1186.

[49]. Buettner M, Bode U. Stromal cells directly mediate the re-establishment of the lymph node compartments after transplantation by cxcr5 or ccl19/21 signalling. Immunology. 2011; 133(2): 257–269. [PubMed: 21426341]

[50]. Benezech C, Mader E, Desanti G, Khan M, Nakamura K, White A, et al. Lymphotoxin-beta receptor signaling through nf-kappab2-relb pathway reprograms adipocyte precursors as lymph node stromal cells. Immunity. 2012; 37(4):721–734. [PubMed: 22940098]

[51]. Yan A, Avraham T, Zampell JC, Aschen SZ, Mehrara BJ. Mechanisms of lymphatic regeneration after tissue transfer. PLoS One. 2011; 6(2):e17201. [PubMed: 21359148]

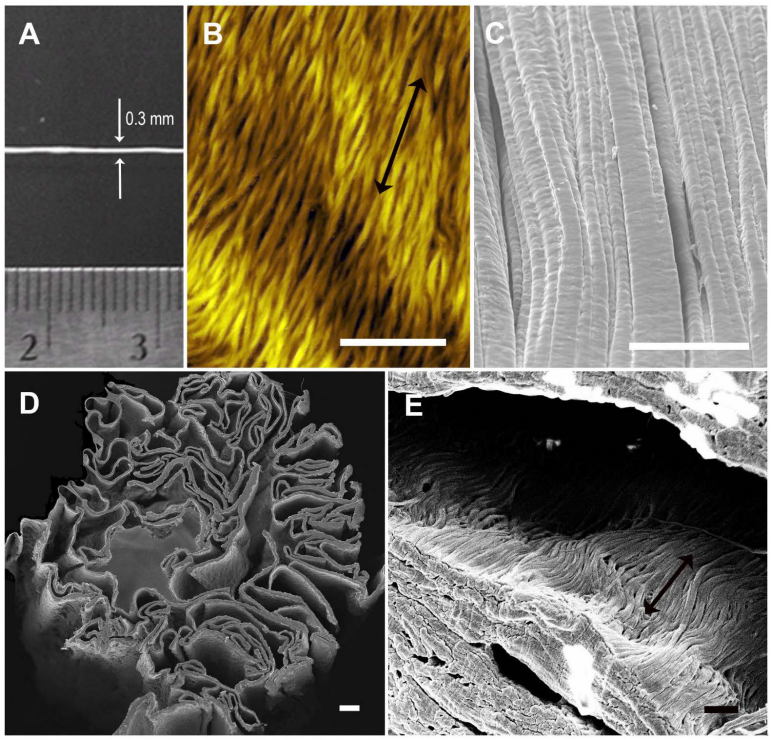

Fig. 1. Characterization of thread-like nanofibrillar collagen scaffolds

A. Macroscopic view of a scaffold prior to *in vivo* implantation. B. Atomic force microscopy imaging of the ultrathin unfolded collagen ribbon formed by aligned collagen fibrils. C. Scanning electron microscopy (SEM) showing the surface of a thread-like collagen scaffold (folded ribbon) with typical pattern of aligned crimped collagen fibrils. D. SEM of the three-dimensional cross-section of the thread-like scaffold. E. SEM showing lumen of the thread-like scaffold having aligned collagen fibrils. Double-head arrows denote orientation of nanofibrils. Scale bars: 1 μm (B); 50 μm (C); 20 μm (D); 1 μm (E).

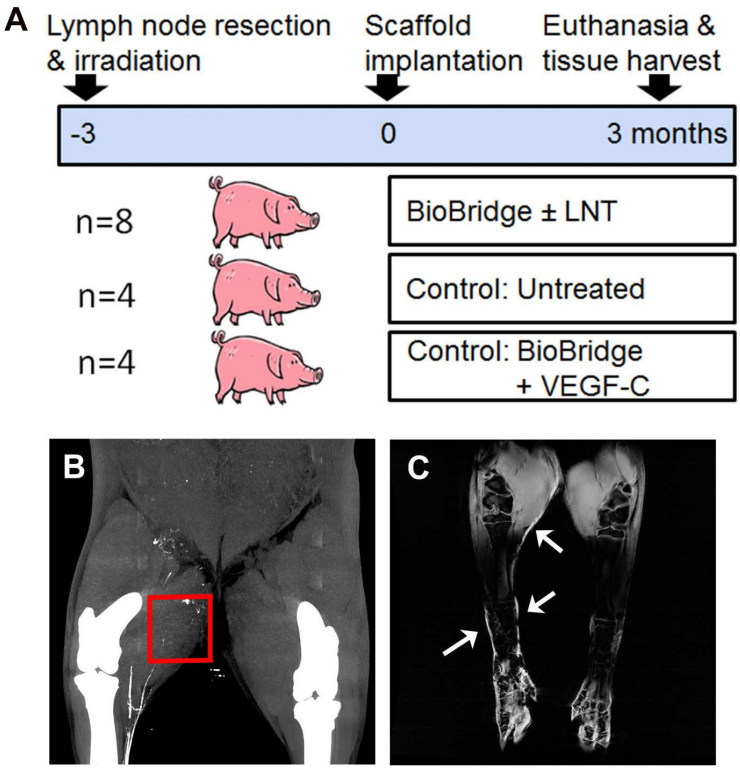

Fig. 2. Outline of porcine lymphedema study

A. Schematic outline of experimental design with time line. B. CT-scan of an untreated animal model at the 3 month time point. Note that the collectors of the thigh are interrupted distally to the area of surgical resection/irradiation (arrow). C. T2-weighted magnetic resonance imaging of a control (untreated control group of the lymphedema model) at the 0 month time point showing asymmetric subcutaneous fluid accumulation or dermal backflow (arrows) as an indirect sign of lymphedema.

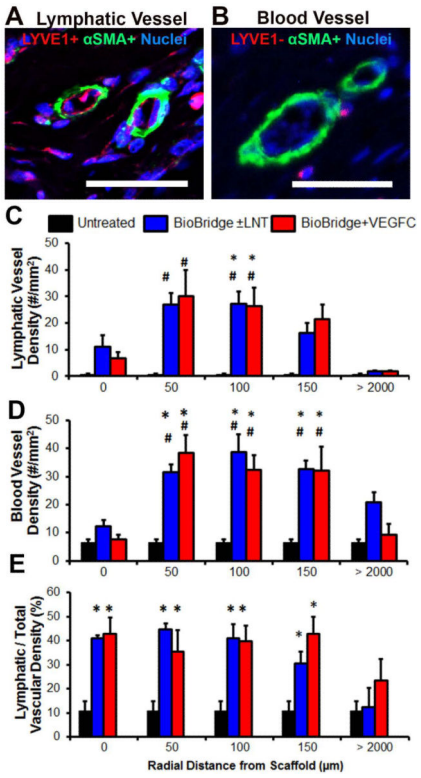

Fig. 3. Immunohistochemistry analysis of lymphatic and blood vascular regeneration

A–B. Confocal microscopy images of immunofluorescently stained (A) lymphatic collectors ($LYVE1^+$, α-SMA^+) and (B) blood-vascular arterioles ($LYVE1^-$, α-SMA^+) in the lymphedematous right limb [24]. Scale bar, 50 μm. C–D. Quantitative analysis (#/mm^2) of the density of (C) lymphatic collectors and (D) blood-vascular arterioles within regional rings, as defined by indicated radial distances from the border of the scaffold. E. Lymphatic fraction of total (blood + lymphatic) vascular density in percent ($n \geq 3$). *$p < 0.05$ *versus* untreated irradiated tissue (control group), $^{\#}p < 0.05$ *versus* surrounding irradiated tissue at > 2000 μm for the same animal, based on ANOVA with Holm's post adjustment.

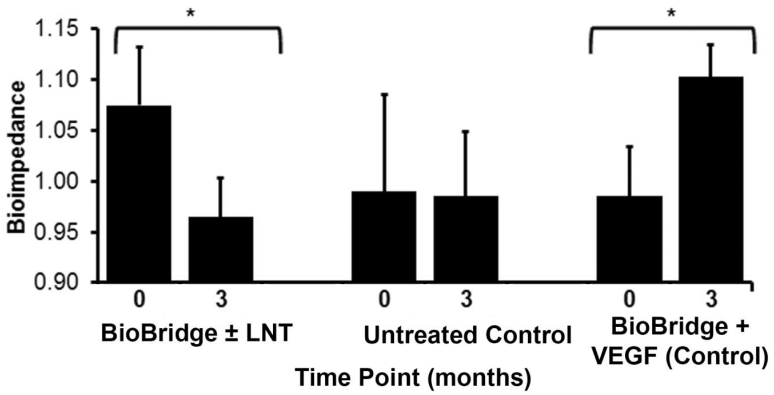

Fig. 4. Changes in the average bioimpedance ratio for each group at initiation of the therapy (0 months) and end of follow up (3 months)

Shown are the mean (column) and the standard error of mean (bar) where *$p < 0.05$ ($n \geq 4$) based on a paired t-test. Increasing bioimpedance is proportional to increasing interstitial water content, and a bioimpedance ratio ≥1.05 is considered pathologic.